Tunnelling and Underground Space Technology 171 (2026) 107482

Contents lists available at ScienceDirect

Tunnelling and Underground Space Technology incorporating Trenchless Technology Research

journal homepage: www.elsevier.com/locate/tust

Short-term surface settlements induced by EPBM twin tunnelling in saturated sandy soils

Binh Thanh Le [a,*], Sam Divall [a], Tra Nguyen [b], Michael C.R. Davies [a,c]

[a] Department of Engineering, School of Science & Technology, City St George's, University of London, London, UK
[b] Vietnam Aviation Academy, Ho Chi Minh city, Viet Nam
[c] School of Engineering and Informatics, University of Sussex, Brighton, UK

ARTICLE INFO

Keywords:
Tunnelling
Case studies
EPBM
TBM
Ground displacement

ABSTRACT

This paper presents a case study of the construction of a 781-metre-long twin-tunnel, using an Earth Pressure Balance Machine (EPBM), in saturated sandy soils in Ho Chi Minh City, Vietnam. The depths of the tunnels were between 11.4m and 24.6m below the ground surface. The averaged trough width and length parameters were 0.326 and 0.446, which are consistent with previous studies in sands. The volume losses ranged from the anticipated levels of less than 0.5% to notably high values reaching up to 2.44%. Low volume losses were associated with areas of dense soil and effective tail void grouting. The characteristics of effective tail void grouting observed in dense sand in this project were grouting pressures close to porewater pressure, coupled with stable grouting volume that was approximately 130% of the volume of the theoretical tail void for the majority of the drive. However, in very loose sandy soil zones it was observed that even very high tail void grout volume did not prevent large settlements. Soil relative density proved to be an influential factor in ground surface vertical displacement, with large magnitudes occurring mainly in loose soil. A threshold relative density $I_d \approx 0.4$ divides the normal volume loss of less than 0.7% range, and that of considerably larger volume loss. The results emphasised the need for caution when tunnelling at shallow depth in loose soil, where the combination of low relative density and shallow cover can result in significant ground movements.

1. Introduction

While numerous studies have been carried out on tunnelling-induced ground movements, relatively few provide comprehensive data and analyses on both soil properties and tunnel boring machine operational parameters (Michalski et al., 2024; Wan et al., 2017a, 2017b; Xu and Bezuijen, 2024). Therefore, reporting of well-documented case studies that address this shortfall is a pressing need.

This paper contributes to addressing that need by presenting and analysing field data from the construction of a twin-tunnel in saturated sandy soils. The case study offers a detailed record of TBM operational parameters, soil conditions, tunnel depth, and their combined influence on ground surface vertical displacements. The following sections present the relevant background to tunnelling operations, followed by the case study and field data. The data is then used for the analyses of the observed ground surface vertical displacement in traverse and longitudinal direction, and the key factors affecting these. These include operational parameters of the Earth Pressure Balance Machine (EPBM), soil relative density, and tunnel depth.

2. Background

2.1. The ground surface vertical displacement induced by tunnelling

Prior to tunnel construction, ground surface vertical displacements are normally predicted using the well-established Gaussian curve approximation (Peck, 1969), as shown below.

$$w = w_{max}\exp(-\frac{y^2}{2i_y}) \quad (1)$$

$$i_y = z_0 K_y \quad (2)$$

where w: ground surface vertical displacement.

y: traverse distance from the tunnel centreline.

* Corresponding author.
E-mail address: b.le@citystgeorges.ac.uk (B.T. Le).

https://doi.org/10.1016/j.tust.2026.107482
Received 10 September 2025; Received in revised form 18 December 2025; Accepted 15 January 2026
Available online 27 January 2026

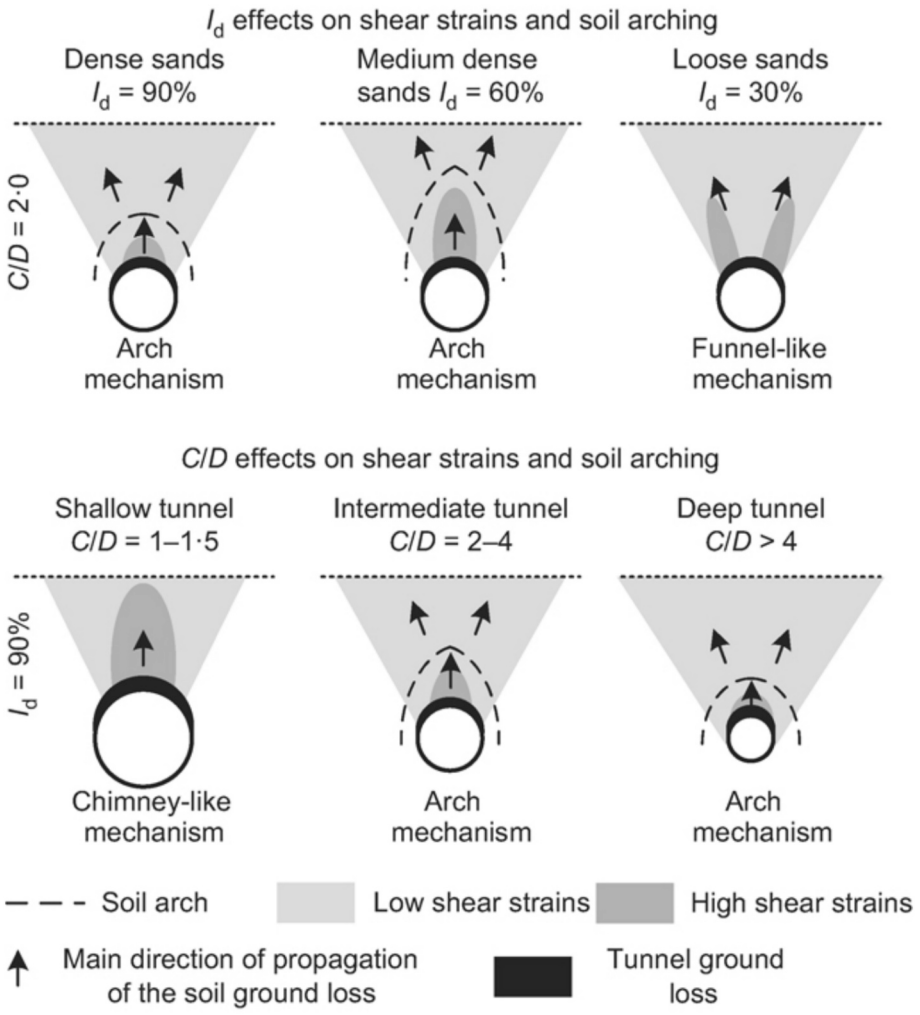

Fig. 1. The effects Id and C/D on soil strains, arching mechanism and ground loss propagation (Franza et al., 2019).

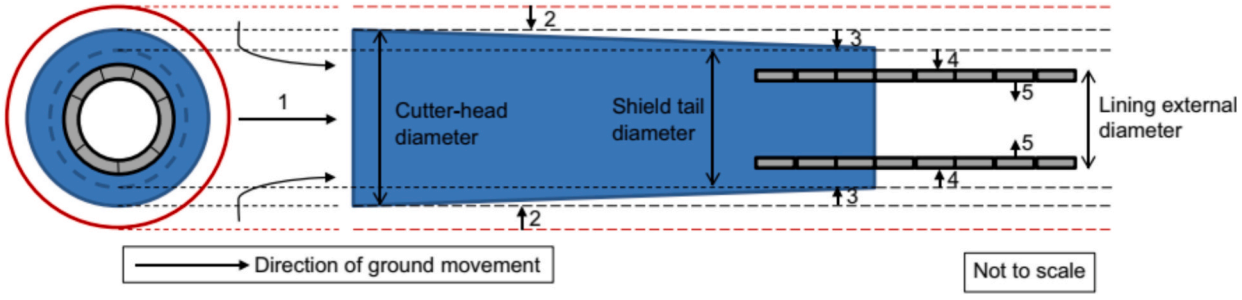

Fig. 2. Illustration on components of volume loss (Wan et al., 2017b).

Table 1
Properties of soil layers (after Le et al., 2021).

Layer	$\gamma\ (kN/m^3)$	$c'(kPa)$	$\varphi'(^\circ)$	Average$SPT\,(N)$	$E\,(MPa)$	$k\,(m/s)$	$D_{50}(mm)$
Fill	19	10	25	N/A	10	10^{-6}	N/A
AC2	16.5	0	24	2	3	10^{-9}	N/A
AS1	20.5	0	30	5	20.8	10^{-7} to 10^{-5}	0.11 *to* 0.75
AS2	20.5	0	33	15	35.5	10^{-7} to 10^{-5}	0.11 *to* 0.9
DC	21	10	22	34	106.5	10^{-8}	N/A
	Water table: 2 m below ground level (bgl).						

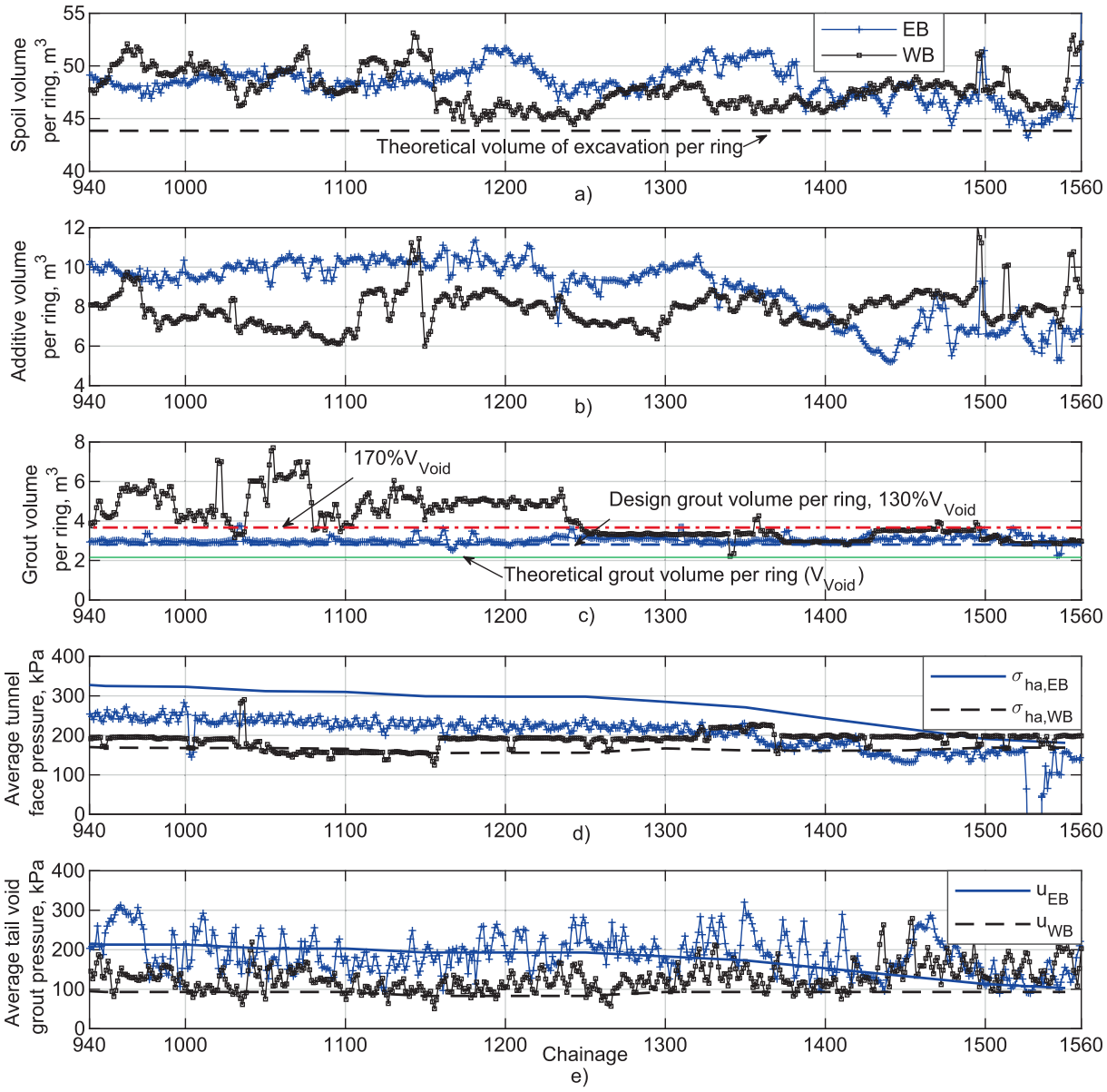

Fig. 3. EPBM operational parameters, three-ring rolling average.

w_{max}: maximum ground surface vertical displacement normally occurs at $y = 0$, i.e above the tunnel centreline.
i_y: traverse distance from the tunnel centreline to the inflexion point of the settlement trough.
z_0: depth from the ground surface to the tunnel centreline.
K_y: trough width parameter in traverse direction.

The value of K_y depends on the geological conditions (Leca and New, 2007; Mair, 2008). For sandy soils, K_y values ranging from 0.25 to 0.45 were observed (Fargnoli et al., 2013; Hu et al., 2020; Mair and Taylor, 1997; Michalski et al., 2024). The results showed that deeper tunnels had wider settlement troughs, while higher volume losses resulted in narrower settlement trough. Ng et al. (2024) reported that K_y generally increased with decreasing relative density, I_d, which contradicted Zhou (2015)'s observation that the surface settlement trough was narrower in looser sands. However, extensive data from Franza et al. (2019) suggested a non-linear relationship between I_d and tunnel depth with K_y in traverse direction.

In the longitudinal direction, Attewell and Woodman (1982) found that the ground surface vertical displacement above the tunnel centreline, w_x, at a distance x from the tunnel face can be described by the cumulative probability function $G()$ as below.

$$w_x = w_{max}\left\{G\left(\frac{x - x_i}{i_x}\right) - G\left(\frac{x - x_f}{i_x}\right)\right\} \quad (3)$$

where $i_x = K_x z_0$ with K_x is the settlement trough length parameter.

x_i: tunnel initial position.
x_f: tunnel face position.
$G(n)$: cumulative distribution function evaluated for n from statistical tables.

2.2. Behaviours of sandy soils subject to tunnelling

The two key characteristics of sandy soil's response to tunnelling are i) soil arching which resists the soil movement above the excavated areas; and ii) the contraction and dilation due to shearing.

Soil arching occurs when adjacent ground zones move relative to each other, e.g. settlement directly above a tunnel heading, causing a

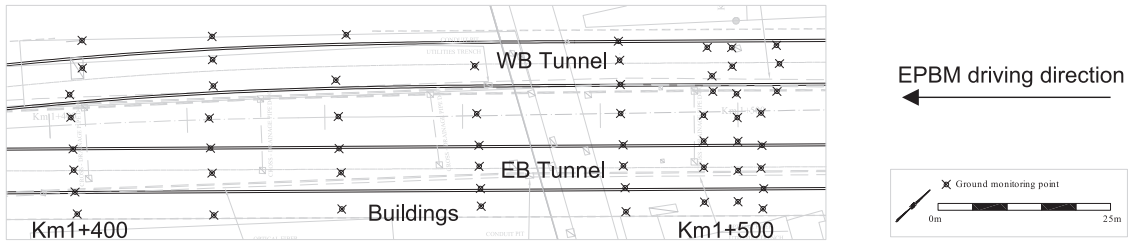

a) Chainage 1400 to 1500

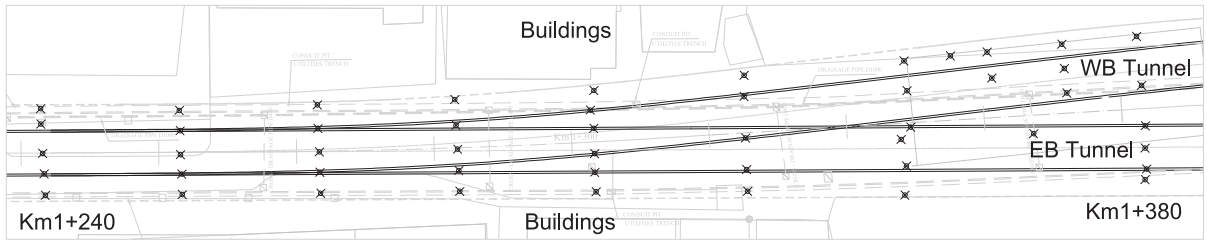

b) Chainage 1240 to 1380

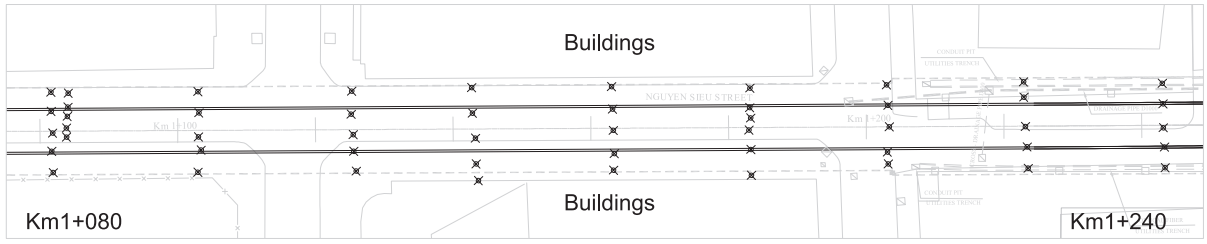

c) Chainage 1080 to 1240

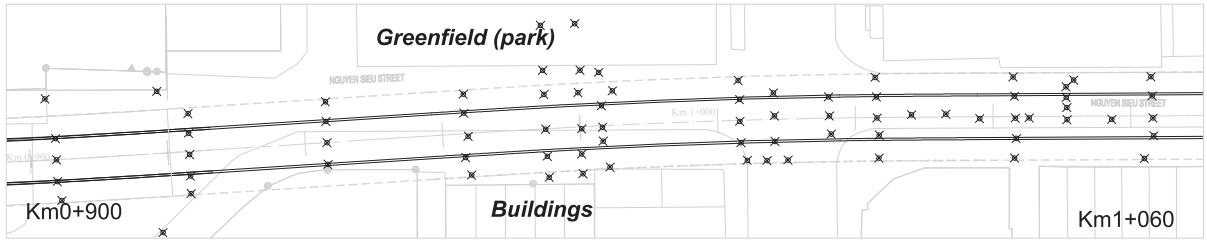

d) Chainage 900 to 1060

Fig. 4. Layout of ground surface vertical displacement along the tunnel route.

redistribution of stresses and rotation of principal stresses, a phenomenon referred to as "stress arching" (Liu et al., 2024). While stress arching results from relative displacements, it does not necessarily form a visible arch in the displacement field. When the deformation pattern develops an actual arch-shaped zone, it is termed "deformation arching", which provides support and contributes to reduce ground deformations. In this paper, the term soil arching refers specifically to "deformation arching".

Soil arching could have a significant influence on tunnelling-induced displacement mechanisms in sands (Franza et al., 2019; Hu et al., 2020). Soil arching is responsible for the variation in the extent of the displacement field with tunnel depth C/D and volume loss V_L; the variation of settlement profile with soil relative density, I_d. The expected deformation-arching patterns at ultimate state for varying overburden depths and soil relative density is presented in Fig. 1. The increase of I_d and the overburden depth leads to stronger arching effects (Iglesia et al., 2013; Liu et al., 2022; Liu et al., 2024).

As the arching is solely maintained by shear stress in soil, any effects that diminish the effective stress, such as seepage, vibration or cyclic loading, will weaken the arching effects (He et al., 2025; Liu et al., 2025; Shibayama et al., 2010). Reduction in arching effect leads to the increase in the ground displacement and hence the volume loss.

Due to the contraction and dilation behaviours, the ground volume loss, at ground surface level, and tunnel volume loss tend to be different in sandy soils. Extensive centrifuge tests revealed that soil contraction was dominant for low volume loss ($V_L \leq 1\%$), meaning ground volume loss was larger than tunnel volume loss (Franza et al., 2019; Marshall et al., 2012; Zhou et al., 2014).

In this paper, the ground volume loss at the surface is used for analyses and discussion. The volume loss can be divided into five subcomponents (Wan et al., 2017b) as depicted in Fig. 2.

Component 1 is corresponding to ground movement in front of the boring machine face occurs as soil moves into the excavation chamber during tunnelling (Xu and Bezuijen, 2019). Components 2 and 3 results in displacements along the tunnel boring machine shield results from the annular gap created by over-cutting of the excavation diameter and shield tapering (if applicable). Component 4 is related to ground movements associated with the closure of the annular void behind the tunnel boring machine shield. Component 5 corresponds to lining deformation due to stresses from surrounding soils. As construction-related ground surface vertical displacement is the main focus, this

Table 2
Summary of the trough width and length parameters.

Tunnel	Chainage	$z_0(m)$	$w_{max}(mm)$	$V_L(\%)$	Trough width parameters		Trough length parameters				$\frac{K_x}{K_y}$
					K_y	$i_y(m)$	K_x	$i_x(m)$	$x(m)$ where $\frac{w}{w_{max}} = 0.5$	$\frac{w}{w_{max}}(\%)$at $x = 0$	
EB	1283	−22.53	−1.14	0.06	0.32	7.13	N/A	N/A	N/A	N/A	N/A
EB	1442	−16.27	−15.4	0.52	0.30	5.0	0.40	6.6	10.7	5.1	1.32
EB	1462	−15.77	−6.5	0.19	0.27	4.3	0.94	14.8	13.8	17.5	3.43
EB	1483	−15.44	−4.28	0.16	0.34	5.31	N/A	N/A	N/A	N/A	N/A
EB	1495	−15.12	−13.6	0.42	0.29	4.5	0.53	8.0	7.1	18.8	1.81
EB	1523	−13.92	−34.4	0.94	0.29	4.0	0.39	5.4	7.3	9.1	1.36
WB	963	−12.66	−12.9	0.35	0.31	4.0	0.70	8.9	11.9	9.0	2.24
WB	975	−12.46	−11.8	0.34	0.34	4.2	0.49	6.0	9.8	5.3	1.43
WB	980	−12.38	−13.5	0.40	0.33	4.1	0.49	6.1	11.0	3.5	1.48
WB	983	−12.36	−14.4	0.42	0.35	4.3	0.38	4.7	10.0	1.7	1.11
WB	1003	−12.25	−20.1	0.48	0.28	3.5	0.32	3.9	8.5	1.5	1.13
WB	1023	−12.07	−10.8	0.34	0.38	4.6	0.50	6.0	7.6	10.1	1.31
WB	1043	−11.94	−26.5	0.71	0.33	3.9	0.35	4.2	10.6	0.6	1.07
WB	1051	−12.01	−16.3	0.40	0.29	3.5	0.50	6.0	10.2	4.4	1.69
WB	1063	−12.04	−20.6	0.55	0.32	3.8	0.33	4.0	9.3	1.0	1.04
WB	1082	−11.79	−72.3	1.94	0.33	3.9	0.38	4.5	4.7	15.0	1.15
WB	1084	−11.80	−79.4	2.04	0.32	3.7	0.34	4.0	7.4	3.4	1.08
WB	1103	−11.89	−89.1	2.44	0.33	4.0	0.37	4.4	7.8	3.8	1.11
WB	1125	−11.69	−78.8	1.93	0.31	3.6	0.39	4.6	6.9	6.5	1.28
WB	1143	−11.60	−65.2	1.60	0.31	3.6	0.30	3.4	7.8	1.2	0.96
WB	1163	−11.60	−41.9	1.10	0.33	3.8	0.32	3.7	7.7	1.8	0.97
WB	1183	−11.55	−27.3	0.80	0.37	4.3	0.39	4.5	7.1	5.7	1.05
WB	1203	−11.56	−21.3	0.57	0.34	3.9	0.39	4.5	10.2	1.2	1.16
WB	1264	−12.22	−6.1	0.18	0.35	4.2	0.53	6.5	15.1	1.0	1.54
WB	1283	−12.36	−12.5	0.31	0.29	3.6	0.48	6.0	12.7	1.7	1.67
WB	1303	−12.17	−20.0	0.55	0.30	3.5	0.45	5.5	12.9	1.0	1.59
WB	1325	−12.46	−8.3	0.25	0.35	4.4	0.36	4.5	14.6	0.1	1.02
WB	1349	−12.01	−23.4	0.73	0.38	4.5	0.43	5.2	5.8	13.0	1.15
WB	1403	−11.40	−28.4	0.71	0.32	3.6	0.35	4.0	11.3	0.2	1.10
WB	1424	−11.44	−18.6	0.67	0.46	5.3	0.71	8.1	10.8	9.0	1.53
WB	1442	−11.71	−6.6	0.19	0.36	4.2	0.68	8.0	14.1	4.0	1.88
WB	1500	−12.65	−24.8	0.56	0.28	3.3	0.33	4.2	3.7	18.9	1.19
WB	1505	−12.60	−29.5	0.70	0.28	3.5	0.32	4.1	3.7	18.1	1.16
WB	1523	−12.48	−17.2	0.52	0.35	4.4	0.48	6.0	4.0	25.1	1.36

paper only considers Components 1, 2, 3 and 4 from the case study.

3. The metro line Ben Thanh-Suoi Tien in Ho Chi Minh city, Vietnam

The tunnel driving direction was from Ba Son station to the Opera House Station. The East Bound (EB) tunnel was completed on 31st October 2017. The EPBM was then dismantled and transported back to the Opera House station for the West Bound (WB) tunnel construction, which completed on 29th June 2018. The tunnels arrangement changed from parallel, offset, and stacked configurations with the depth varied from $\approx 11.4m$ to $\approx 24.6m$ when they went from Ba Son station to the Opera House station, which was in a more crowded area. Further details can be found in Le et al. (2023).

3.1. The site geology

The Soil Investigation Report (Le et al., 2023) showed that the water table was approximately 2 m below the ground level and the soil strata (Fig. 5b) consisted of five main layers. Their properties are presented in Table 1. The D_{50} values stated in Table 1 are for a range of Particle Size Distribution curves conducted from samples taken at different depths within the layer. The descriptions of the soil layers can be seen below.

Fill: The topsoil is mainly fill materials including sand, clay, gravel, brick, concrete.
AC2 (Alluvial clay): The soil material is homogenous, very soft fat CLAY.
AS1 (Alluvial sand): The main component of this layer is silty fine SAND. In general, the soil is very loose to loose.
AS2 (Alluvial sand): The main component of this layer is medium to coarse SAND and the density is from medium dense to dense sand with occasional loose pockets.
DC (Diluvium clay): The material consists of homogeneous, hard to very hard, weakly cemented, low permeability, clayey soil.

3.2. Tunnel Construction

3.2.1. The EPBM and tunnel lining

In this project, the EPBM had the length 8.5 m with the shield outer diameter 6.79 m. The tunnel lining had outer and inner diameters 6.65 m and 6.05 m, respectively. With the excavation diameter 6.82 m and the ring nominal length 1.2 m, the theoretical volumes of excavation and the tail void were 43.84m^3 and $V_{void} = 2.16m^3$ per ring, respectively. The tail void was filled with grout to minimise the closure of the ground.

3.2.2. EPBM operational parameters

Since the EPBM operational parameters are referenced in subsequent sections, this section presents an overview of the recorded values. Given the inherent fluctuation in the field data, Fig. 3 presents three-ring rolling average values for better clarity. The spoil volume consisted of the excavated soils, including ground water, mixed with additives (acrylic polymer and bentonite) (Fig. 3a). The volume of spoil, measured by a magnetic flow meter, was consistently larger than the theoretical excavation volume. This was attributed to the additional volume of material resulting from additives being injected into the EPBM chamber as well as an increase in voids ratio of the excavated material (i.e. “bulking”). The volume of additives is depicted in Fig. 3b. At the area around chainage 1500, the spikes in the volume of additives and the spoil volume (Fig. 3a), measured independently, affirms the confidence of the measurements.

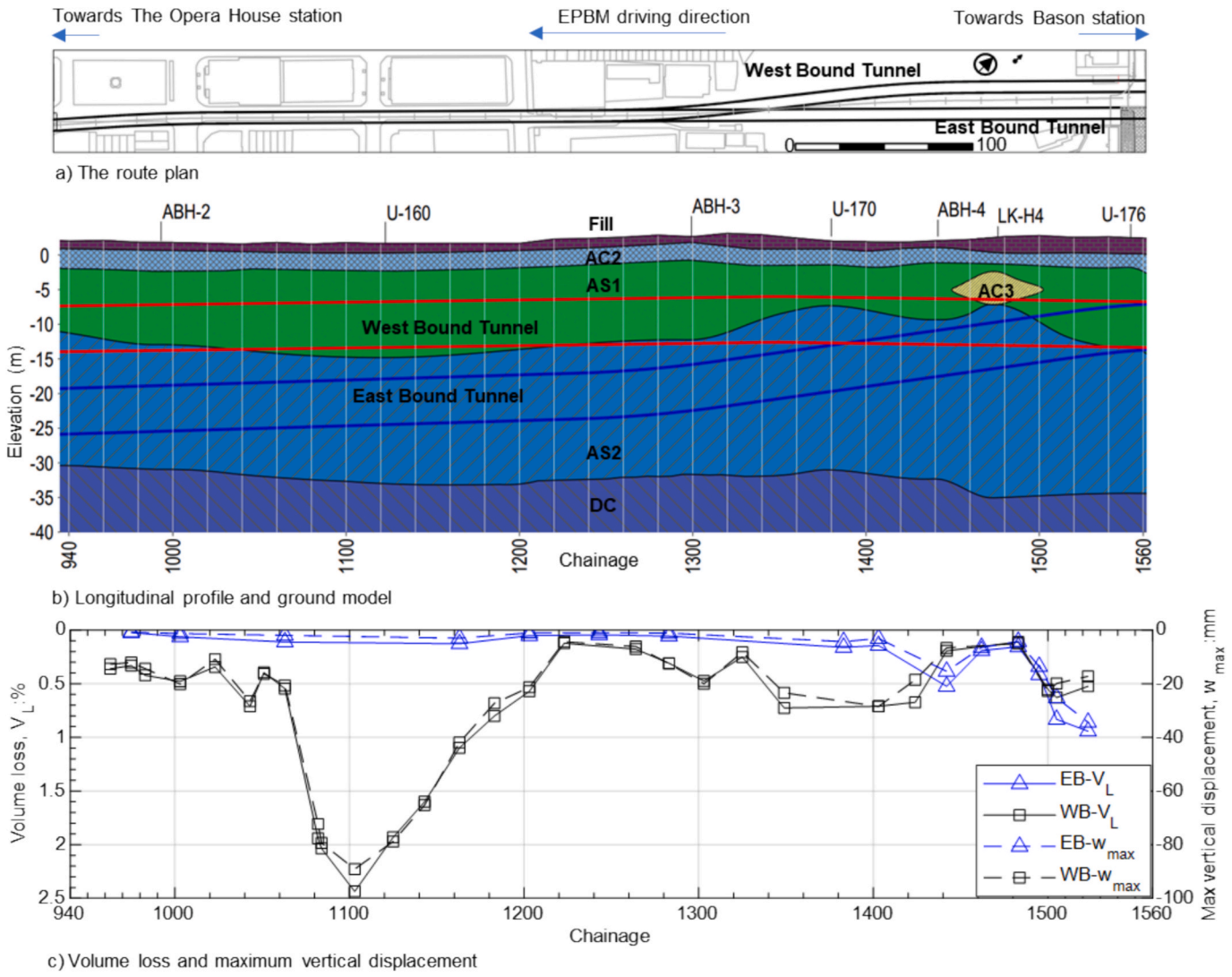

Fig. 5. The tunnel route, ground model, and surface vertical displacement (after Le et al. (2023)).

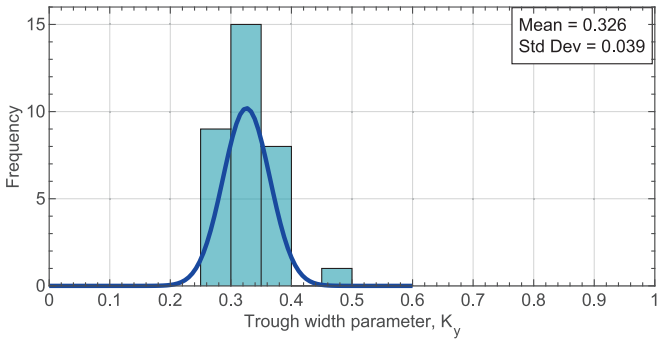

Fig. 6. Histogram of trough width parameter.

The tail void was filled with two-part grout to minimise the closure of the ground. The two-part grout consists of Liquid A and Liquid B. For a 1,000 L grout mix, Liquid A accounts for 920 L typically includes 260 kg of Ordinary Portland Cement, 35 kg of bentonite, 4.8 L of stabilizer, and 819 L of water. Liquid B accounts for 80 L and is sodium silicate. The initial gel time of Liquid A and B was 5 s to 30 s. After approximately 1 h, the strength was at least $0.15N/mm^2$. The measured tail void grout volumes per ring is presented in Fig. 3c. For comparison purpose, also shown are the theoretical tail void volume per ring $V_{void} = 2.16\ m^3$, the design tail void grout volume of $130\%V_{void}$, and the upper bound threshold of $170\%V_{void}$. From chainage 1560 to 1240, the tail void grout volume for both tunnels were similar and relatively stable, with the majority of the grout volumes lying between the theoretical volume V_{void} and the threshold $170\%V_{void}$. However, from chainage 1240 to 940, the tail void volume for the WB was considerably larger than that for the EB tunnel.

Fig. 3d presents the average tunnel face pressure, measured by two earth pressure sensors at the tunnel axis level, for each ring. Also plotted in the figure for comparison is the predicted active horizontal earth pressure, σ_{ha}, at the tunnel axis where K_a was calculated using appropriate values from Table 1. Fig. 3e presents the average grouting pressures from the two simultaneous grouting pipes together with the hydrostatic pore-water pressure, u, at the injection level which was $\approx 2.747m$ above the EPBM shield axis level (i.e. positioned at angles $\pm 36°$ from the shield vertical axis). It could be seen that overall, for the shallower tunnel, WB, the average grouting pressure was lower than that for the deeper tunnel EB.

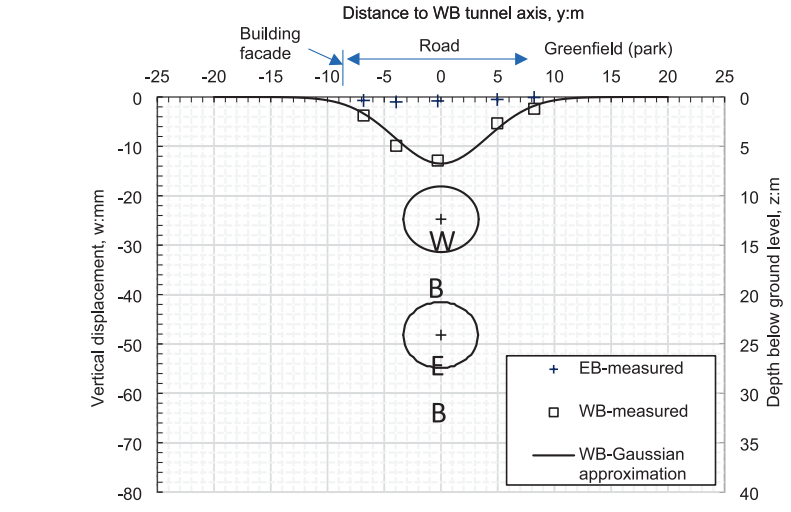

a) Traverse ground surface vertical displacement at chainage 980.

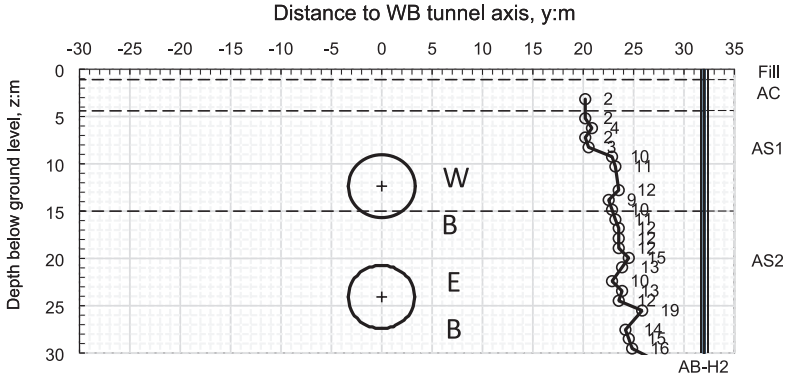

b) Interpreted soil profile, SPT values with depth and tunnels locations at chainage 980.

Fig. 7. Field data at chainage 980.

4. The ground surface monitoring scheme and measurements

4.1. Monitoring scheme overview

Along the tunnel route, the ground surface vertical displacement measurements were taken at the ground monitoring points indicated in Fig. 4. The monitoring sections were arranged approximately perpendicular to the tunnel centreline along the route. A digital level with a resolution of 0.01 mm was used to determine the level of the ground monitoring points. The sign conventions used in this paper are as below.

In longitudinal direction: $-ve\,x$ indicates that the monitoring section was ahead of the EPBM face and $+ve\,x$ indicates the EPBM face had passed the monitoring section.

In traverse direction: $-ve\,y$ indicates the distance from the tunnel centreline of the tunnel to the monitoring points on the left-hand side commensurate with the EPBM driving direction (Fig. 4).

Ground surface vertical displacement: $-ve\,w$ indicates settlement whereas $+ve\,w$ indicates heave.

The measured ground surface vertical displacements were used to derive the least-squares best-fit Gaussian trough at each monitoring sections, providing estimates of volume losses V_L at the ground surface (Fig. 5) and trough width parameters K_y. This paper only presents estimations of V_L and K_y with $R^2 \geq 0.75$ which had the mean value $R^2_{mean} = 0.93$ and standard deviation (SD) $SD_{R^2} = 0.059$. These values are summarised in Table 2 along with key information such as z_0 and the ratio w/w_{max} at $x = 0$. Further discussions on the data are provided in relevant sections.

4.2. Ground surface settlement measurements

Fig. 5 presents the overview of the measured ground surface vertical displacements, the ground surface volume loss together with the ground model along the tunnel route. The following sections discuss the extent of the settlement trough in traverse direction, longitudinal settlement, which followed by the magnitude of the settlement.

4.3. Traverse surface settlement

4.3.1. Statistics of settlement trough width

The settlement trough width K_y values at different locations along the tunnel route are summarised in Table 2. Fig. 6 presents the distribution of K_y values which ranged from 0.27 to 0.46 with the mean value 0.326 and the standard deviation (SD) $SD_{K_y} = 0.039$. These values are in line with the range from 0.25 to 0.45 previously reported in the literature, e.g. Fargnoli et al. (2013) and Mair and Taylor (1997).

4.3.2. The effect of building on settlement trough shape

As the project was in a congested urban area, most of the twin tunnel route was underneath existing roads, with buildings on the two sides. Buildings inherently increase the ground-structure interface stiffness which tend to widen the surface settlement trough induced by tunnelling. This widening effect is inversely proportional to the distance between the building to the tunnel centreline, indicated by the ratio e/L, where e is the eccentricity and L is the building length. For a building with $\frac{e}{L} = 0.8$ and $V_L = 0.5\%$, the surface settlement trough has been

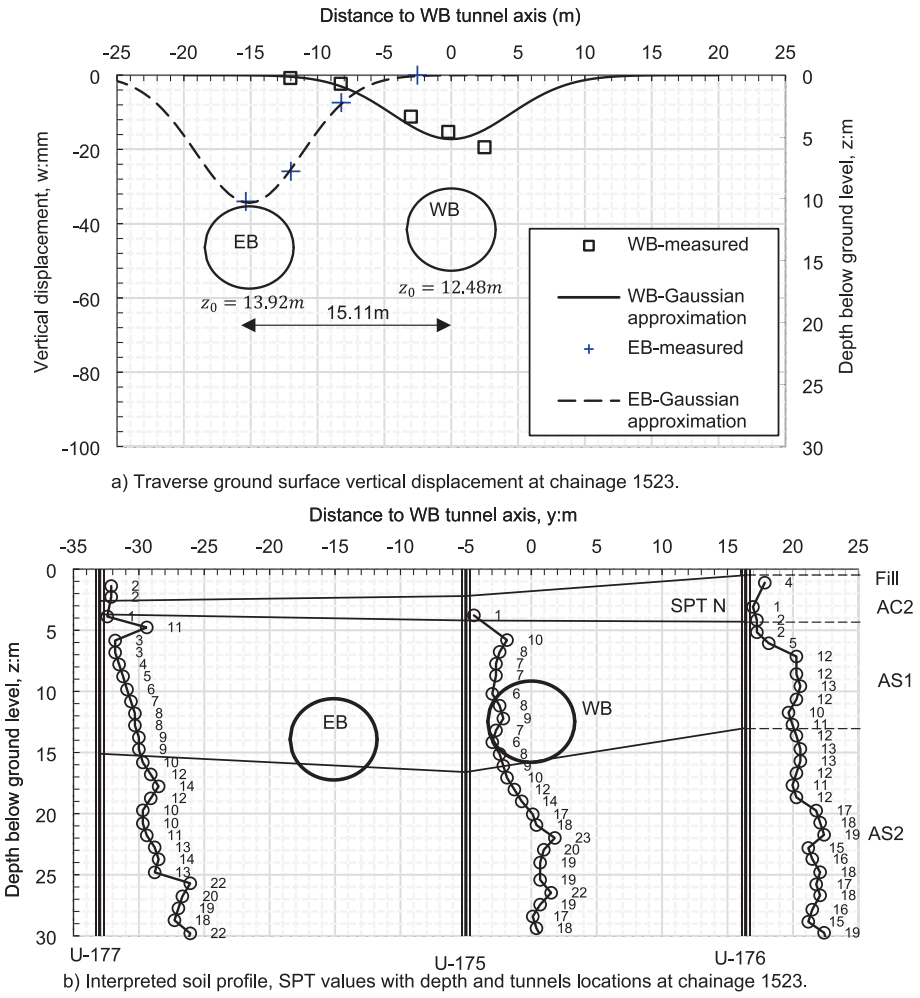

Fig. 8. Field data at chainage 1523.

observed to be similar to that in greenfield condition (Ritter et al., 2017).

In this project, most buildings had $\frac{e}{L} > 0.8$. To examine the effect of the buildings on the traverse surface settlement trough, Fig. 7 presents the trough at chainage 980. The right-hand side area was a park and could be considered as greenfield, whereas the left-hand side area consisted of buildings (see Fig. 4d for the site layout). The buildings had lengths $L \approx 18m$ with eccentricities $e \approx 17m$ give the ratio $\frac{e}{L} \approx \frac{17}{18} \approx 0.94$. Even with only 5 useable monitoring points at this section, it could be said that the buildings, with large e/L, did not have considerable effect on the tunnelling-induced ground surface vertical displacement trough.

4.3.3. The effect of previous tunnel to settlement trough shape

At chainage 1523, the two tunnels, 15.11 m apart and at similar depths, offered an opportunity to investigate the effect of construction sequence on the trough shape. Fig. 8a presents the traverse ground surface vertical displacements induced by the EB and WB tunnels, respectively. The limited number of the monitoring points prevents a detailed quantitative assessment on the effect of construction sequence to the trough shape. Nevertheless, for the latter tunnel WB, the settlement trough was asymmetrical. The alignment of the EB and WB tunnels near chainage 1523 were relatively straight – i.e. there is no effect from EBPM steering – and, as can be seen from Fig. 8b, the soil SPT-N profiles have very similar values. Therefore, the asymmetry could be attributed to the previously injected tail void grout from the EB tunnel that could have strengthened the soil in area to the left of the WB tunnel, which in turn, caused the asymmetry of the settlement trough (Divall et al., 2017).

4.3.4. The effects of relative density to settlement trough width

As previously discussed in the Background section, observations have indicated a complex relationship between K_y and relative density I_d. Cubrinovski and Ishihara (1999) proposed a method for estimating relative density, I_D, using the following equation:

$$I_D = 21\left(\frac{N}{\frac{\sigma'_v}{98} + 0.7}\right)^{\frac{1}{2}} \tag{4}$$

where N is the SPT value

σ'_v is vertical effective stress.

Eq. (4) does not consider the grain size effect which can be considered by

$$I_d = \left\{\frac{N\left(0.23 + \frac{0.06}{D_{50}}\right)^{1.7}}{9}\left(\frac{98}{\sigma'_v}\right)^{\frac{1}{2}}\right\}^{\frac{1}{2}} \tag{5}$$

In this paper **Eq. (5)** is used, unless otherwise stated, to calculate the average I_d from the tunnel centreline to the top of the sandy soil AS1, where D_{50} was obtained from the particle size distribution curves. The Appendix A provides data from a borehole with relevant calculations for I_d at chainage 1103. Table 3 presents the I_d, from boreholes mostly within 20 m radius off the tunnel centreline, together with values of C/D, V_L, K_y in this project and those from other case studies for

Table 3
Relationship of I_d, C/D, K_y and..V_L

No	z_0	C/D	V_L(%)	K_y	I_d	Project & note
1	22.5	2.9	0.06	0.32	0.44	Ho Chi Minh city line 1, EB-1283
2	16.3	1.9	0.52	0.30	0.40	Ho Chi Minh city line 1, EB-1442
3	13.9	1.6	0.94	0.29	0.34	Ho Chi Minh city line 1, EB-1523
4	12.4	1.4	0.40	0.33	0.52	Ho Chi Minh city line 1, WB-980
5	11.9	1.3	2.44	0.33	0.30	Ho Chi Minh city line 1, WB-1103
6	11.7	1.3	1.93	0.31	0.30	Ho Chi Minh city line 1, WB-1125
7	11.6	1.2	1.60	0.31	0.30	Ho Chi Minh city line 1, WB-1143
8	12.2	1.3	0.55	0.30	0.43	Ho Chi Minh city line 1, WB-1303
9	12.5	1.4	0.25	0.35	0.43	Ho Chi Minh city line 1, WB-1325
10	11.4	1.2	0.71	0.32	0.40	Ho Chi Minh city line 1, WB-1403
11	11.7	1.3	0.19	0.36	0.42	Ho Chi Minh city line 1, WB-1442
12	12.5	1.4	0.52	0.35	0.44	Ho Chi Minh city line 1, WB-1523
13	10.5	1.2	0.58	0.44	0.70	Milan underground line 1
14	10.9	1.2	0.64	N/A	0.70	extension (Migliazza et al., 2009)
15	11.5	1.3	0.54	0.40	0.70	Consistent I_d across the sites were
16	11.6	1.3	0.57	N/A	0.70	reported
17	11.9	1.4	0.54	N/A	0.70	
18	12.3	1.4	0.43	N/A	0.70	
19	12.7	1.5	0.43	N/A	0.70	
20	13.1	1.6	0.34	N/A	0.70	
21	13.4	1.6	0.36	0.34	0.70	
22	13.8	1.7	0.38	N/A	0.70	
23	15.3	1.1	0.20	0.45	0.49	Chainage 4150, Line 9 of the Barcelona Metro (Yubero and Bonet, 2024) $I_d \approx 0.49$, estimated using Equation (4) with the data at chainage 4150.
24	15.0	1.7	0.27	N/A	0.70	Milan underground line 5 (
25	15.0	1.7	0.82	N/A	0.70	Fargnoli et al., 2013) I_d ranged from 0.4 to 0.9, no detailed I_d for each site was reported, the average I_d is used in this paper.

comparison purposes in the later sections.

Fig. 9 depicts the relationship between K_y and I_d compiled from Table 3. The scattered data points highlight the complex relationship between K_y and I_d, as K_y depends on various factors. However, a few comparisons with the previous studies can be drawn as below.

From Fig. 9, for similar values of I_d (e.g., in the range of $I_d \approx 0.4$ and $I_d \approx 0.7$), there appears to be no clear correlation between the C/D ratio with K_y. This contrasts with the findings of Franza et al. (2019) who reported that a higher C/D ratio generally corresponds to a wider surface settlement trough. The discrepancy between the field observation from this paper and experimental results above could be attributed to two main factors, as discussed below.

First, Franza et al. (2019) assessed the trough width under the condition of similar volume losses, whereas Fig. 9 reflects measurement taken after the construction, where volume losses varied. Second, the field conditions, as in the case studies shown in the figure, involve complex geology (e.g. layered soils), different construction techniques, and potentially ground water effects, with the latter not being present in centrifuge modelling in uniform dry sand. Therefore, K_y prediction requires further studies.

4.4. Longitudinal surface settlement

The normalised longitudinal ground surface vertical displacements are depicted in Fig. 10, which appears crowded but it serves the purpose of presenting the overall pattern of the development of the ground surface volume loss in relation to the TBM advancement. For clarity, the later sections present longitudinal ground surface vertical displacements at typical sections.

For most of the monitoring sections the vertical displacement, w, started to stabilise when the EPBM passed the monitoring section at approximately a distance of $x_f \geq 2z_0$. Other case studies of tunnelling in sandy soils reported similar observations that the ground surface vertical displacement still developed even when $x_f \geq z_0$ (Fargnoli et al., 2013; Michalski et al., 2024; Migliazza et al., 2009; Withers, 2001).

4.4.1. Trough length parameter

Fig. 11 presents the distribution of the trough length parameters, K_x (Table 2), of the longitudinal ground surface vertical displacements, which were estimated using the cumulative distribution function (Attewell and Woodman, 1982; Hu et al., 2020). The K_x values ranged from 0.3 to 0.94, with the mean value $K_x = 0.446$, and the standard deviation $SD_{K_x} = 0.14$. The distribution of K_x (Fig. 11) was wider than that for K_y (Fig. 6), reflected by the larger standard distribution $SD_{K_x} = 0.14 > SD_{K_y} = 0.039$.

The ratio K_x/K_y ranges from 0.96 to 3.43 with most of the values are around 1 to 1.5 with the mean value of 1.386 and the standard deviation of 0.382 (Table 2**)**. This further corroborates observation from Wongsaroj et al. (2006) which reported K_x/K_y ratios were mostly larger than unity for tunnelling in sandy soils. A possible reason for $K_x > K_y$ may be attributed to soil arching in the longitudinal direction, where stress redistribution along the tunnel axis could lengthen the settlement trough. However, further experimental evidence is needed to validate this hypothesis.

4.4.2. Total and components of ground surface settlement

Figs. 5c and 10 provides an overview of the total ground surface and its components across all monitoring sections. Overall, the total ground surface vertical displacements induced by the shallower WB tunnel were noticeably larger than those of the deeper EB tunnel (Fig. 5c). For most

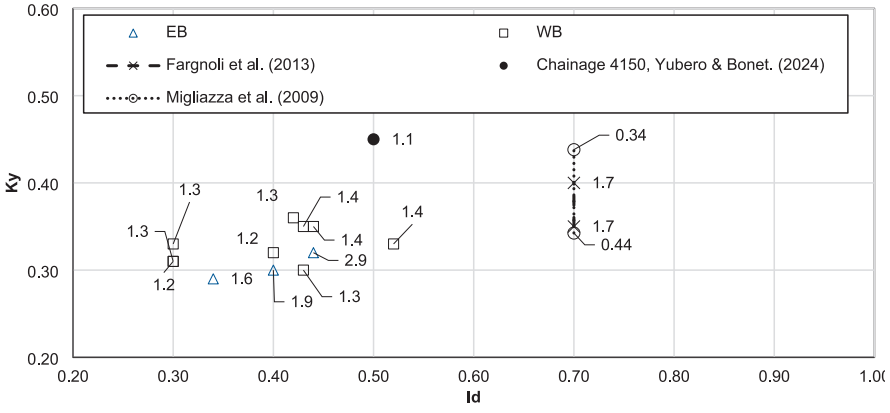

Fig. 9. Relationship between and.

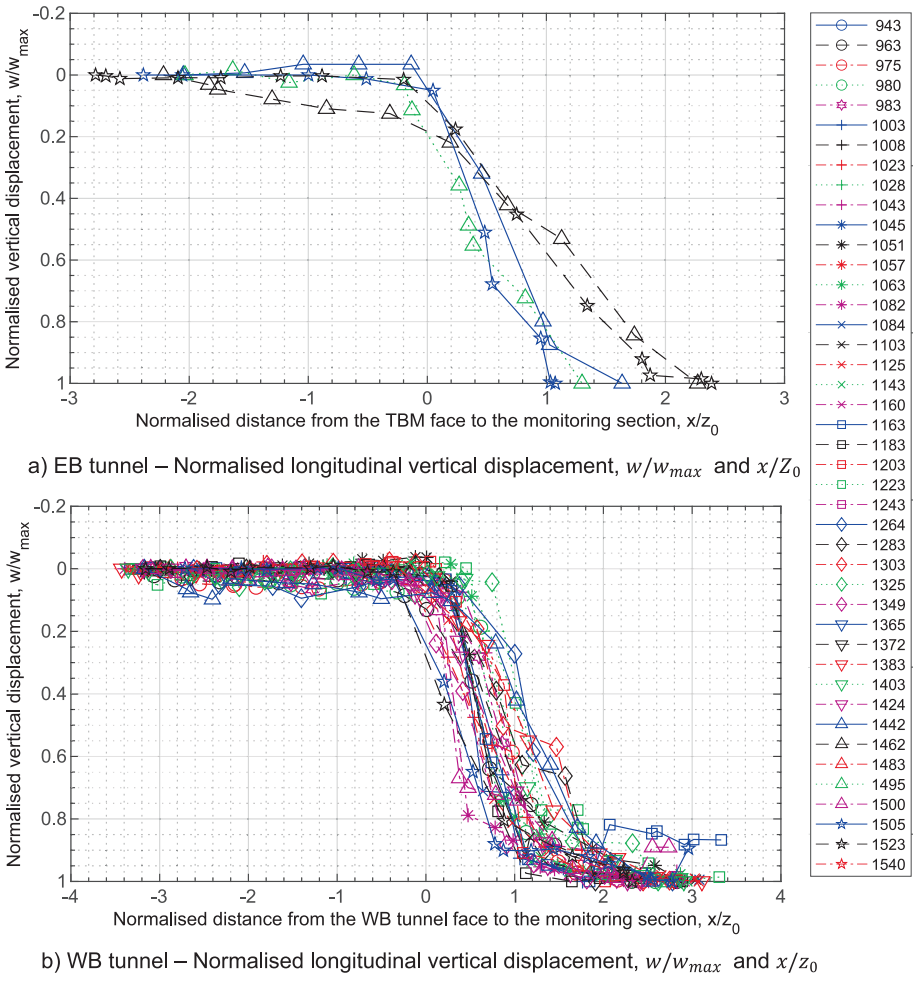

Fig. 10. Maximum vertical displacement above tunnel centreline.

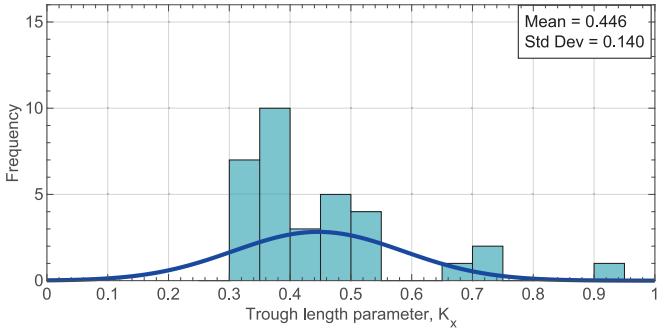

Fig. 11. Histogram of trough length parameter.

of the route, the total settlement and volume loss were $w < 30mm$ and $V_L < 1\%$ which are expected for well-controlled EPBM tunnelling (Michalski et al., 2024).

Regarding the components of the ground surface settlement, Fig. 12 offers a more detailed breakdown of a typical composition, at chainage 1103, for improved clarity. Consistent with findings in sandy soils reported by Migliazza et al. (2009) and Withers (2001), Component 1 only accounted for less than 10% of the total settlement across most of the section.

Small Component 1 is often attributed to the tunnel face support pressure. For WB tunnel where the face pressure exceeded the active horizontal stress σ_{ha}, such limited surface vertical displacement was expected. However, the EB tunnel also exhibited small Component 1 displacement, despite the tunnel face pressure was consistently 20 −35% below σ_{ha} (Fig. 3d). This suggests that ground arching mechanisms (as shown in Fig. 1) may have stabilised the soil, thereby limiting ground surface vertical displacement in front of the tunnel face.

As the EPBM progressed, the combined effects of excavation-induced vibrations and disturbance from high-pressure grouting may have weakened the soil arching effect. As a result, the magnitude of ground surface vertical displacements and volume loss during the passage of the EPBM (Components 2&3), and during the tail void grouting (i.e. Component 4) increased in magnitude (Fig. 10 and Fig. 12a). The increase in ground surface vertical displacements after the EPBM face were most evident during the construction of the WB tunnel from chainage 1240 to 940 (Fig. 5), with the maximum settlement occurred at chainage 1103. At this location, w reached up to $\approx 95mm$ with $V_L \approx 2.44\%$, which were significantly larger than that for the EB tunnel at this location, and for the rest of the route. To investigate this, the EPBM operational parameters (Fig. 3) and soil properties of the nearby boreholes (Fig. 12b) are used for analysis.

From chainage 1240 to 940, the volume of tail void grout for the EB tunnel remained stable. However, for the WB tunnel, the tail void grout volume was significantly higher than the threshold of $170\%V_{void}$ yet the volume losses were considerably larger than those for the EB tunnel (Figs. 3c and 5c). This implied, for WB tunnel, some amount of the tail void grout volume penetrated through the pores of loose sand. The phenomenon was most evident in the vicinity of chainage 1103 where grout penetration was seen at the ground surface during the construction the WB tunnel. Verification confirmed that the tail void penetration

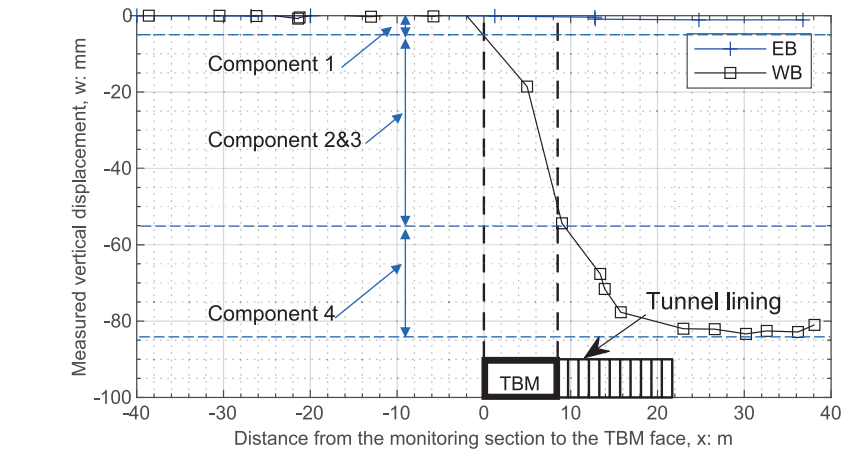

a) Longitudinal ground surface vertical displacement at chainage 1103.

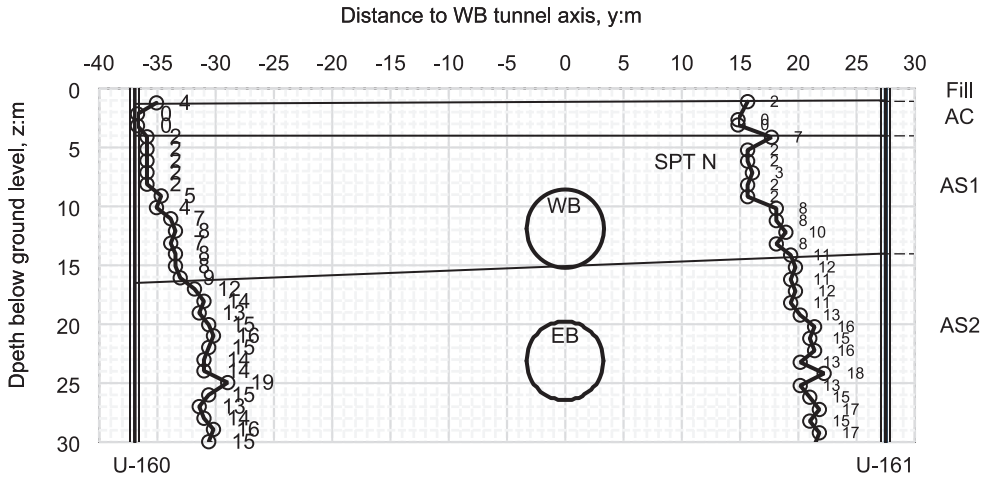

b) Interpreted soil profile, SPT values with depth and tunnels locations.

Fig. 12. Field data at chainage 1103.

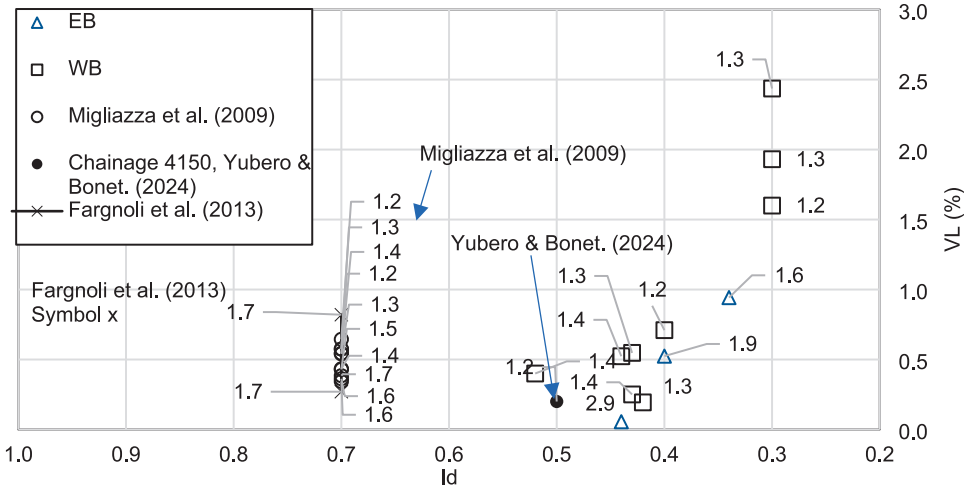

Fig. 13. Relationship between, and.

occurred through soil pores and not through any unfilled boreholes. The higher the volume of the tail void grout penetrated through the sandy soil led to the greater reduction in grouting effectiveness.

In addition to EPBM parameters, other important factors that influences ground volume loss, V_L, are soil relative density I_d, and tunnel depth C/D. From Fig. 12, the shallower WB tunnel, positioned in the looser soil, reflected by the lower SPT-N values, induced larger V_L. To gain a clearer insight into the relationship between I_d, C/D, and V_L, the next section compares these data from this project and other case studies for further analyses.

4.5. The effects of relative density, tunnel arrangement to ground surface volume loss

Franza et al. (2020), based on data from centrifuge tests and case studies, suggests general relationships that volume loss, V_L, is inversely proportional to tunnel depth C/D ratio, and soil density, I_d. Their case studies did not consider loose sand nor stacked tunnels, which are both characteristic of this project.

To examine the relationship between V_L, C/D, and I_D, Fig. 13 presents relevant data from this project and other case studies. The scattered data is due to the complexity of tunnel construction. This includes many variables such as geology between sites and case studies, interpolation/extrapolation of the soil properties from the borehole locations to the monitoring sections, EPBM types and technology, and construction sequence. Notwithstanding this, three key observations on the effects of I_d, C/D, and tunnel construction sequence to V_L can be drawn.

First, in this case study the data (Figs. 7, 8 and 13) suggests that the tunnel arrangement (whether parallel, inclined or stacked) does not significantly influence the volume loss generated by the second tunnel. Overall, the volume losses associated with the WB tunnel (i.e. the second bored tunnel) shows no clear trend and remained within the typical range of volume losses expected which were less than 0.71%.

Second, for tunnelling in loose sand with $I_d < 0.4$, I_d reduction leads to sharp increase of V_L. High V_L are often associated with a weak arching effect which is inherent in loose sandy soil. In addition, loose sandy soil has high liquefaction potential, implying a high possibility of further soil loosening around the tunnel lining which can lead to high volume loss (Le et al. 2023, and Shirlaw and Boone 2023). On the other hand, for tunnelling in medium dense to dense sand ($I_d > 0.4$) in which soil arching effect is stronger, V_L is generally less than 0.7%. For $I_d \geq 0.4$, the effect of I_d to V_L is less apparent.

Third, with $I_d > 0.4$ and of similar values, V_L is inversely proportional to C/D, most clearly seen at Migliazza et al. (2009) data. A higher C/D ratio corresponds to increased effective stress which enhances the arching effect, contributing to a reduction in ground displacements and V_L. These observations offer a quantitative perspective on the influence of I_d to V_L.

5. Conclusions

This paper presents the field monitoring data and relevant analyses of the ground surface vertical displacements from the construction of the 781 m long twin-tunnels using an EPBM in saturated sandy soils in Ho Chi Minh City, Vietnam.

The trough width parameter, K_y, was found to be 0.326 on average, consistent with previous studies in sands. The trough length parameters, K_x, had a mean value of 0.446 and typically K_x was larger than K_y. The mean value of the ratio K_x/K_y was found to be 1.39. This ratio is similar to that reported in previous studies on tunnelling in sand and is different from observations from tunnelling in clay in which $K_x/K_y < 1$. The complexities of tunnel construction hinder a reliable prediction of K_y only based on soil relative density and tunnel depth, and further research on trough width K_y is needed.

The observed volume losses varied widely along the tunnel route, ranging from typical values of less than 0.5% to an abnormally high 2.44%. Ground surface vertical displacements were primarily caused by soil movements during EPBM passage and tail void grouting, rather than ahead of the tunnel face. The study highlights the impact of grouting effectiveness on controlling tunnelling-induced vertical ground surface displacements behind the tunnel face. Adequate grouting pressures close to porewater pressures, coupled with stable grouting volumes around the designed 130% of theoretical void, helped minimise vertical ground surface displacements in dense sands. However, in the very loose sandy soil zones, even injecting over 170% of theoretical grouting volumes could not prevent – or might have exacerbated – large ground surface settlements. These findings highlight that tail void grouting alone cannot compensate for soil with low relative density. Based on evidence from physical modelling and case studies, soil relative density, I_d, is an influential factor on tunnelling-induced ground movements and needs to be considered in tunnel construction.

Overall, dense sandy soils exhibiting arching effects tended to show smaller ground surface displacements compared to loose sandy soils under similar shear conditions due to tunnelling. This reduced displacement at the ground surface may be associated with greater dilatancy, i.e. increase in volumetric strain in dense sands whereas loose sands typically undergo more contractive volumetric strain during shearing.

The threshold relative density $I_d = 0.4$ divides the "high" and "low" range of volume loss. For denser soil with $I_d \geq 0.4$, which benefits from more pronounced arching effects, in most of the cases the volume loss was less than 0.7%, and was inversely proportional to the tunnel depth C/D ratio. For soil with $I_d < 0.4$, reduction of I_d led to sharp increase in volume loss, especially for shallow tunnel, e.g. $C/D \approx 1.2-1.6$ as observed in this project.

For practical applications, caution is essential when tunnelling at shallow depths in loose sandy soils. The relative density of the soil, I_d, can be estimated using commonly available data such as vertical effective stress, SPT N-values, and D_{50}. When tunnelling in sandy soils with $I_d < 0.4$, this study recommends: i) considering appropriate ground improvement measures prior to construction; and ii) closely monitoring tail void grout parameters during construction, as excessively large grout volumes may be counterproductive.

Effective control of tunnelling-induced ground surface settlement in sandy soils requires a holistic approach: maintain adequate grouting pressure near porewater pressure, ensure stable grout volumes, and account for soil relative density conditions.

CRediT authorship contribution statement

Binh Thanh Le: Writing – original draft, Visualization, Software, Methodology, Funding acquisition, Formal analysis, Data curation, Conceptualization. **Sam Divall:** Writing – review & editing, Validation, Funding acquisition. **Tra Nguyen:** Visualization, Software, Investigation, Formal analysis, Data curation. **Michael C.R. Davies:** Writing – review & editing, Validation, Conceptualization.

Declaration of competing interest

The authors declare that they have no known competing financial interests or personal relationships that could have appeared to influence the work reported in this paper.

Acknowledgements

This research is funded by Vietnam National Foundation for Science and Technology Development (NAFOSTED) under grant number 107.04-2020.31. This research was also supported by the Global Challenges Research Funding provided by Research England. The field data is indispensable to this research and thanks are due to Mr. Y. Ishihara, Mr. M. Kuroki from the General Consultant, and Dr. Q. Phan, Mr. N. Nguyen, Mr. C. Vo from the contractors for their valuable inputs.

Appendix A. Supplementary data

Supplementary data to this article can be found online at https://doi.org/10.1016/j.tust.2026.107482.

Data availability

Data will be made available on request.

References

Attewell, P.B., Woodman, J.P., 1982. Predicting the dynamics of ground settlement and its derivitives caused by tunnelling in soil. Ground engineering 15.

Cubrinovski, M., Ishihara, K., 1999. Empirical correlation between SPT N-value and relative density for sandy soils. Soils Found. 39, 61–71. https://doi.org/10.3208/SANDF.39.5_61.

Divall, S., Goodey, R.J., Stallebrass, S.E., 2017. Twin-tunnelling-induced changes to clay stiffness. Géotechnique 67, 906–913. https://doi.org/10.1680/JGEOT.SIP17.P.151.

Fargnoli, V., Boldini, D., Amorosi, A., 2013. TBM tunnelling-induced settlements in coarse-grained soils: the case of the new Milan underground line 5. Tunn. Undergr. Space Technol. 38, 336–347. https://doi.org/10.1016/j.tust.2013.07.015.

Franza, A., Marshall, A.M., Zhou, B., 2019. Greenfield tunnelling in sands: the effects of soil density and relative depth. Geotechnique 69, 297–307. https://doi.org/10.1680/JGEOT.17.P.091.

Franza, A., Marshall, A.M., Zhou, B., Shirlaw, N., Boone, S., 2020. Greenfield tunnelling in sands: the effects of soil density and relative depth. Geotechnique 70, 639–646. https://doi.org/10.1680/JGEOT.19.D.002.

He, J., Liao, S., Liu, C., Liu, H., Cui, J., Liu, Y., 2025. Investigation on tunnel face failure under varying seepage conditions in saturated sand using coupled CFD-DEM and analytical modelling. Comput. Geotech. 183, 107232. https://doi.org/10.1016/J.COMPGEO.2025.107232.

Hu, X., He, C., Lai, X., Walton, G., Fu, W., Fang, Y., 2020. A DEM-based study of the disturbance in dry sandy ground caused by EPB shield tunneling. Tunn. Undergr. Space Technol. 101, 103410. https://doi.org/10.1016/J.TUST.2020.103410.

Iglesia, G.R., Einstein, H.H., Whitman, R.V., 2013. Investigation of soil arching with centrifuge tests. J. Geotech. Geoenviron. Eng. 140, 04013005. https://doi.org/10.1061/(ASCE)GT.1943-5606.0000998.

Le, B.T., Nguyen, N.T., Divall, S., Goodey, R.J., Taylor, R.N., 2021. Modified gap method for prediction of TBM tunnelling-induced soil settlement in sand-a case study, in: Geotechnical Aspects of Underground Construction in Soft Ground. CRC Press, pp. 584–589.

Le, B.T., Nguyen, T.T.T., Divall, S., Davies, M.C.R., 2023. A study on large volume losses induced by EBPM tunnelling in sandy soils. Tunn. Undergr. Space Technol. 132, 104847. https://doi.org/10.1016/J.TUST.2022.104847.

Leca, E., New, B., 2007. Settlements induced by tunneling in Soft Ground. Tunn. Undergr. Space Technol. 22, 119–149. https://doi.org/10.1016/j.tust.2006.11.001.

Liu, M.-B., Xiao, J.-H., Liao, S.-M., Liu, Z.-Y., He, J.-Z., Men, Y.-Q., Sun, J.-C., 2025. Model test on the effects of shield machine cutterhead vibration on tunnel face stability in sandy ground. Underground Space 22, 39–54. https://doi.org/10.1016/J.UNDSP.2024.04.009.

Liu, Q.W., Wang, H.L., Chen, R.P., Yin, Z.Y., Lin, X.T., Wu, H.N., 2022. Effect of relative density of 2D granular materials on the arching effect through numerical trapdoor tests. Comput Geotech 141, 104553. https://doi.org/10.1016/J.COMPGEO.2021.104553.

Liu, X.Y., Franza, A., Jimenez, R., 2024. Effects of relative density and dilatancy on stress and deformation arching of sand over an active trapdoor. Comput. Geotech. 173, 106485. https://doi.org/10.1016/J.COMPGEO.2024.106485.

Mair, R.J., 2008. Tunnelling and geotechnics: new horizons. Geotechnique 58, 695–736. https://doi.org/10.1680/geot.2008.58.9.695.

Mair, R.J., Taylor, R.N., 1997. Bored tunnelling in the urban environment, in: Fourteenth International Conference on Soil Mechanics and Foundation Engineering. 14th ICSMGE (Hamburg) Conference 19. Vol 4, pp. 2353–2380.

Marshall, A.M., Farrell, R., Klar, A., Mair, R., 2012. Tunnels in sands: the effect of size, depth and volume loss on greenfield displacements. Géotechnique 62, 385–399. https://doi.org/10.1680/geot.10.P.047.

Michalski, A., Branque, D., Berthoz, N., Rallu, A., Mohamad, W., Szymkiewicz, F., Le Kouby, A., Bourgeois, E., 2024. Greenfield response to EPBM tunneling in paris and relations with TBM operation variables. J. Geotech. Geoenviron. Eng. 150. https://doi.org/10.1061/JGGEFK.GTENG-12136.

Migliazza, M., Chiorboli, M., Giani, G.P., 2009. Comparison of analytical method, 3D finite element model with experimental subsidence measurements resulting from the extension of the Milan underground. Comput. Geotech. 36, 113–124. https://doi.org/10.1016/j.compgeo.2008.03.005.

Ng, C.W.W., Wong, A.Y.Y., Buenaventura, A.D.F., Zhu, P.Y., 2024. Three-dimensional numerical analysis of twin tunnelling in two-layered soil strata. Tunn. Undergr. Space Technol. 153, 106028. https://doi.org/10.1016/J.TUST.2024.106028.

Peck, R.B., 1969. Deep excavations and tunneling in soft ground. Proc. 7th ICSMFE 225–290.

Ritter, S., Giardina, G., Dejong, M.J., Mair, R.J., 2017. Influence of building characteristics on tunnelling-induced ground movements. Geotechnique 67, 926–937. https://doi.org/10.1680/JGEOT.SIP17.P.138.

Shibayama, S., Izawa, J., Takahashi, A., Takemura, J., Kusakabe, O., 2010. Observed behaviour of a tunnel in sand subjected to shear deformation in a centrifuge. Soils Found. 50, 281–294. https://doi.org/10.3208/SANDF.50.281.

Shirlaw, J.N., Boone, S.J., 2023. A study on large volume losses induced by EBPM tunnelling in sandy soils, B.T. Le, T.T.T. Nguyen, S. Divall, M.C.R. Davies. Tunnelling and Underground Space Technology 142, 105424. https://doi.org/10.1016/J.TUST.2023.105424.

Wan, M.S.P., Standing, J.R., Potts, D.M., Burland, J.B., 2017a. Measured short-term ground surface response to EPBM tunnelling in London Clay. Geotechnique 67, 420–445. https://doi.org/10.1680/JGEOT.16.P.099.

Wan, M.S.P., Standing, J.R., Potts, D.M., Burland, J.B., 2017b. Measured short-term subsurface ground displacements from EPBM tunnelling in London Clay. Geotechnique 67, 748–779. https://doi.org/10.1680/JGEOT.SIP17.P.148.

Withers, A.D., 2001. Surface displacements at three surface reference sites above twin tunnels through the Lambeth Group. In: Building Response to Tunnelling: Case Studies from Construction of the Jubilee Line Extension, 37. Thomas Telford Publishing, London, pp. 735–754.

Wongsaroj, J., Borghi, F.X., Soga, K., Mair, R.J., Sugiyama, T., Hagiwara, T., Bowers, K. H., 2006. Effect of TBM driving parameters on ground surface movements: Channel Tunnel Rail link Contract 220. In: Geotechnical Aspects of Underground Construction in Soft Ground. Taylor & Francis Group, London, pp. 335–341.

Xu, T., Bezuijen, A., 2024. Monitoring and data analyses of pressure changes and ground settlements induced by slurry TBM tunneling in a semiconfined aquifer: case study in the Netherlands. J. Geotech. Geoenviron. Eng. 150, 05024013. https://doi.org/10.1061/JGGEFK.GTENG-12434.

Xu, T., Bezuijen, A., 2019. Bentonite slurry infiltration into sand: filter cake formation under various conditions. Geotechnique 69, 1095–1106. https://doi.org/10.1680/jgeot.18.P.094.

Yubero, M.T., Bonet, E., 2024. Ground Surface Effect of Earth Pressure Balance Tunnelling in Deltaic Deposits: A Case Study of Line 9 of the Barcelona Metro. Sustainability 16, 8275. https://doi.org/10.3390/SU16188275.

Zhou, B., 2015. Tunnelling-induced ground displacements in sand (PhD thesis). University of Nottingham.

Zhou, B., Marshall, Alec.M., Yu, H.-S., 2014. Effect of Relative Density on Settlements above Tunnels in Sands, in: Tunneling and Underground Construction. American Society of Civil Engineers, Reston, VA, pp. 96–105. https://doi.org/10.1061/9780784413449.010.